JMEPEG (2012) 21:1254–1259
DOI: 10.1007/s11665-011-0018-x

1059-9495/$19.00

Evaluation of the Fatigue Life of High-Strength Low-Alloy Steel Girth Welds in Aqueous Saline Environments with Varying Carbon Dioxide Partial Pressures

M. Lemos, C. Kwietniewski, T. Clarke, C.J.B. Joia, and A. Altenhofen

(Submitted April 26, 2011; in revised form July 1, 2011)

High-strength low-alloy steel girth weld specimens were subjected to fatigue tests in saline environments saturated with different carbon dioxide partial pressures. As expected, results show that increases in gas concentration initially affect fatigue life adversely, but when higher partial pressures are associated with low stresses, a reduction in the negative impact of environmental conditions is seen. This may be related to a competition between corrosion rates and mechanisms of crack initiation and propagation. Data is presented with the aim of contributing toward the establishment of a database of results in literature which may lead to better understanding of the phenomena involved through association of these with ongoing research.

Keywords API 5L X65 steel, carbon dioxide, girth welds, saline environments, steel catenary risers

1. Introduction

Steel catenary risers (SCRs) are structures of common use in the oil and gas offshore exploration industry (Ref 1-8) which are generally manufactured by girth welding of high-strength low-alloy steel (HSLA) tubes. Of particular interest are those steels conforming with the 5L standard of the American Petroleum Institute (API) (Ref 1, 6, 9), which are generally regarded as cost-effective materials for pipeline construction, and exhibit good weldability and high toughness (Ref 1, 10-12).

It is well-known that SCRs are inevitably subjected to low-frequency dynamic loading caused mainly by vessel movements and water flow-induced motion (Ref 1-5). As a result, the fatigue behavior of these structures is a matter of significant concern.

Girth welds are an especially critical part of the structure due to the high levels of stress concentration which are common in this region. Besides fatigue loading, girth welds are usually subjected to potentially corrosive environments on both the internal and external surfaces (Ref 1-13). Weld caps in contact with seawater are effectively protected by the use of common corrosion-prevention methods (e.g., sacrificial anodes and impressed currents), which means that integrity of this region is less of a concern. Furthermore, due to their widespread use offshore, there is a significant volume of information available in the literature regarding the performance of HSLA steel welds in seawater environment (Ref 1-5). On the other hand, the behavior of SCR girth welds, when in contact with corrosive internal fluids, has received less attention (Ref 1, 3, 8). Apart from saline water, substantial concentrations of carbon dioxide or hydrogen sulfide contribute to the aggressiveness of the internal environment (Ref 3, 14). Thus, it is critical to consider the potential effect of these chemically harsh environments on the fatigue behavior of the internal surface (Ref 1-8). Literature on corrosion resistance of welded HSLA steels in sweet environments (usually sea water with CO_2) shows that preferential corrosion of the weld metal and the heat-affected zone (HAZ) are of particular concern; however, limited experimental data is available to quantify the possible changes in the mechanical behavior of such weld joints in these environments (Ref 3, 4, 7). In addition to the usually more sensitive regions of the weld, it is known that the girth weld toe also acts as a stress concentrator and is a preferential site for fatigue crack nucleation (Ref 15-18).

Corrosion involving CO_2 reactions in steels have been the subject of many studies (Ref 14, 19-25); of the mechanisms described in these, one of the less investigated is the counter-intuitive improvement in fatigue life of specimens subjected to certain combinations of load and aggressive corrosion environments. Several aspects of this phenomenon have been observed and explanations for their occurrence given (Ref 1, 15), but a comprehensive evaluation of the environment and stress conditions under which this occurs has still not been provided. The absence of such data in the literature has also been identified by other authors (Ref 3, 4, 8). Forming a database of results involves performing a substantial amount of laborious tests, and it is thought that such a collection of data needs to be gradually built through collaborative efforts.

In this way, this study aims at contributing to an increase in the available data on fatigue resistance of HSLA steel joints,

M. Lemos, C. Kwietniewski, T. Clarke, and **A. Altenhofen**, Post-Graduation Program in Mining, Metallurgical and Materials Engineering (PPGEM), Federal University of Rio Grande do Sul (UFRGS), Av. Osvaldo Aranha, 99, Sala 610, Porto Alegre, RS, Brazil; and **C.J.B. Joia**, Centro de Pesquisas e Desenvolvimento Leopoldo Américo Miguez de Mello (CENPES)—PETROBRAS, Av. Horácio Macedo, 950, Cidade Universitária, Rio de Janeiro, RJ, Brazil. Contact e-mail: tclarke@demet.ufrgs.br.

through the evaluation of cross sections of API 5L X65 girth welds subjected to four-point bending corrosion-fatigue tests in an environmental chamber containing salted water saturated with different CO_2 partial pressures. Results are presented in the form of stress range against number of cycles to fracture (S-N) curves which are fitted and extrapolated according to ASTM standards (Ref 26, 27).

2. Methodology

Corrosion-fatigue test chambers which allowed control of the test and environmental parameters were designed and assembled (see schematic in Fig. 1). During the test, the specimens remained inside an acrylic chamber and were exposed to distillated and deionized water containing 115,000 ppm of dissolved chloride at a controlled temperature of 35 °C. The test chamber configuration also included a gas injection line, through which the solution was saturated with different partial pressures of carbon dioxide, and an applied load controlling system. Continuous monitoring of pH values of the solution guaranteed that values were constantly in the 4.7 ± 0.2. Test parameters are summarized in Table 1. More details of the test system and its construction and components are described in Ref 1.

Specimens were removed from a girth weld of a 18″ pipe, with a geometry which kept the weld centralized in the supports of the testing rig and ensured exposure of the weld root to the aggressive environment; Fig. 2 shows the weld joint regions and the areas exposed to the environment. As shown in Fig. 3, the specimens were 270-mm long and 30-mm wide, and had a thickness of 14.7 mm. The weld root was not grinded off, which means that stress concentration effects in this region were present in the tests, thus ensuring conditions closer to those encountered in real conditions.

The specimens were protected with a careful painting process, which left only the area of interest exposed. This painting process involved the use of a nonsolvent-based epoxy primer, covered with two thick coatings of zinc epoxy-phosphate paint.

The test was performed using a four-point bending system, thus subjecting the weld root to tension loading. For calculation of the applied load, the cross section of the specimen was considered to have a constant rectangular cross section. Correlations between the applied load and stress were then calculated according to (Ref 28):

$$\sigma = \frac{3}{2}(L - I)\frac{P}{bh^2}, \qquad \text{(Eq 1)}$$

where σ is the tensile stress of the material in MPa, L and I are the distances between the supports of the lower and upper devices, respectively (240 and 80 mm), P is the applied load in N, and b and h are the specimen width and thickness, which are measured for each specimen.

One specimen was instrumented with strain gages in order to confirm the correlation between the load cell readings and the stress transferred to the weld joint. The maximum applied stresses varied from 85 to 35% of the average ultimate tensile strength of the weld, which was obtained previously, through a

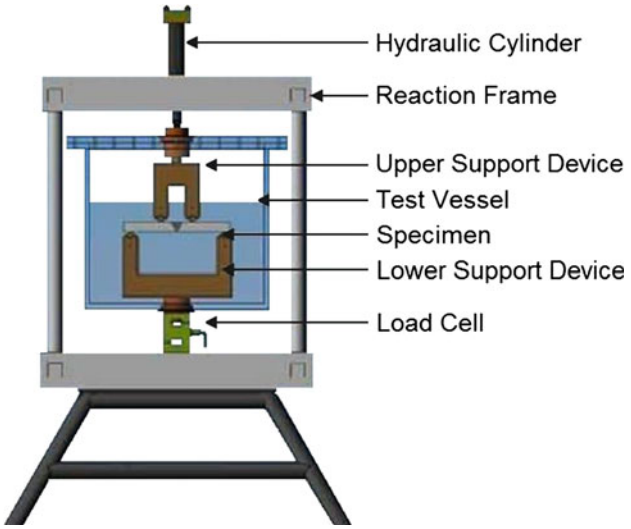

Fig. 1 Test chamber and configuration used during corrosion-fatigue tests

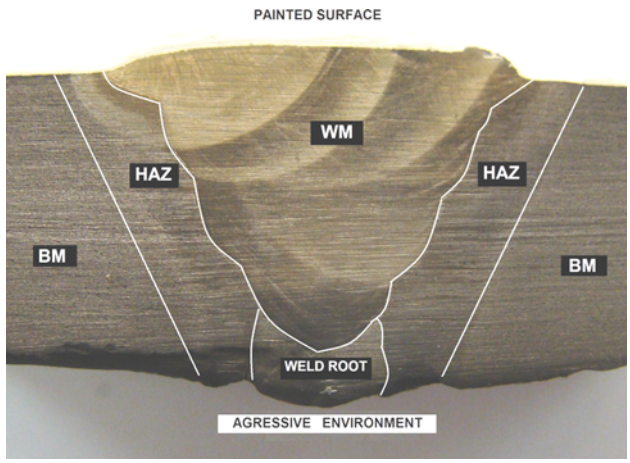

Fig. 2 Girth weld profile showing base metal (MB), heat-affected zone (HAZ), weld metal (WM), and weld root (etched, 10% H_2SO_4 aqueous solution)

Table 1 Fatigue and corrosion-fatigue test parameters

Condition	Gas (N_2 balance)	Partial pressure, kPa	Specimens	Number of stress ranges tested	Frequency, Hz	Days until run-out
1	Air	···	16	6	15	0.77
2	CO_2 99.995%	103	8	4	0.2	57.87
3	CO_2 50%	55	8	4	0.2	
4	CO_2 20%	21	8	5	0.2	

uniaxial tensile test. The load ratio was 0.1 and the run-out for each specimen was 1 million cycles.

Results were plotted on a log-log graph of stress range against the number of cycles until failure (S-N curve). The data presentation on the graph was based on the ASTM E468 standard (Ref 26). In addition, all the equations of the curve fits and the standard deviation calculation for the resulted fatigue data were obtained using methodologies proposed in the ASTM E739 standard (Ref 27). Equations of the fitted curves are presented in the $Y = A + BX$ form, where log $N = Y$, log $\Delta\sigma = X$, and the coefficients A and B are calculated according to the curve fitting procedure established by the standard. Standard errors (θ) for each fit and correlation coefficients (R^2) for each set of data were also calculated according to ASTM E739.

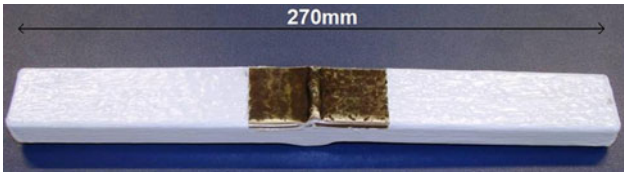

Fig. 3 Corrosion-fatigue tests specimens showing weld root area which was exposed to the environment during tests

Fracture analysis of all specimens were performed in an attempt to identify recurring fracture mechanisms; this was done following standard metallographic procedures.

3. Results

Table 2 shows the chemical analysis of the material of the tubes received from the supplier, which, as expected, is similar to the specifications for API 5L X65 steels.

Corrosion-fatigue tests were divided in four different classes, according to environment parameters. All results from tests are presented in Table 3; this data was used for S-N curve construction, as can be seen in Fig. 4. Table 3 also shows the parameters of the curve fitting procedure, including the calculated standard errors and the correlation coefficients for each set of data. The S-N curve obtained from the results of tests performed in air were used as a reference for the curves of the corrosion-fatigue tests results.

All specimens presented the same fracture aspect, which consisted of crack initiation at the weld root toe, with propagation in the direction perpendicular to the applied stress, as can be seen in Fig. 5. This region consists of a transition between weld metal (from the root bead) and the HAZ. The region of crack initiation is shown in Fig. 6.

Table 2 Results from the chemical composition analysis of the base metal

	Chemical composition (wt.%)										
	C	**Si**	**Mn**	**P**	**S**	**Cr**	**Ni**	**Cu**	**Nb**	**Ti**	**V**
Average	0.14	0.3	1.47	0.021	0.0057	0.023	0.017	0.1	0.045	0.011	0.047
X65 standard	<0.26	<0.45	<1.65	<0.025	<0.03	<0.30	<0.30	<0.2	<0.05	<0.06	<0.08

Table 3 Fatigue and corrosion-fatigue test results

			Curve fit parameters (ASTM E739)			
Condition	**Stress range Δσ, MPa**	**Number of cycles to rupture (*N*)**	***A***	***B***	**θ**	**R^2**
Air	221	751795, 925953, *1000000*(a)	13.58	−3.25	0.11	−0.92
	249	743610, 450718, *1000000*(a)				
	304	422895, 329180, 547016				
	387	155737, 166070, 122918				
	415	90900, 110898, 75782				
	470	75354, 106247, 89006				
21 kPa CO_2	269	614266, 257900, 315151	13.81	−3.4	0.13	−0.72
	296	279388				
	322	157098, 135167				
	403	94099, 97530				
55 kPa CO_2	194	*1000000*(a), *1000000*(a)	13.81	−3.4	0.12	−0.85
	277	202571, 350453, 447862				
	332	178197, 197289				
	415	99003, 61475, 84593				
103 kPa CO_2	178	541645	14.94	−4.04	0.10	−0.94
	257	184236, 212015				
	309	88535, 98155				
	332	42562				
	362	35688, 33991				

(a) Specimen reached run-out (not considered for S-N curve fit)

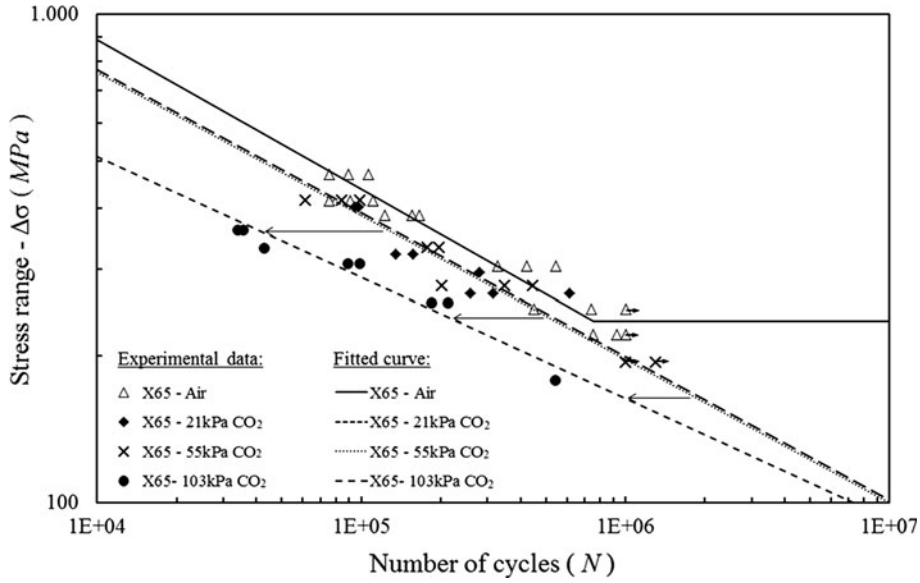

Fig. 4 S-N curves resulting from fatigue in air and corrosion-fatigue tests

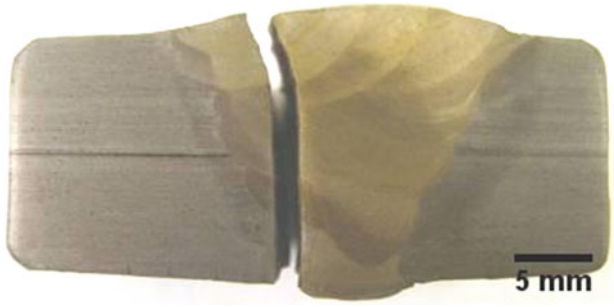

Fig. 5 Typical aspect of fractures of tested specimens (etched, 10% H_2SO_4 aqueous solution)

Fig. 6 Metallography of the region of failure initiation showing the location of the fatigue crack nucleation site. Magnification: 200×. Reagent: NITAL 2%

4. Discussion

It was clear from the tests that fatigue cracks nucleated from the girth weld root toe, which seems to corroborate results described by other authors (Ref 15-18, 29); stress concentration in weld joints is such an important issue that specific standards, such as the British Standard BS 7608, exist as a way of establishing S-N project curves depending on the girth weld geometry (Ref 15, 30). In this way it is clearly evident that microstructure plays a secondary role in fatigue failure steps (Ref 18, 30, 31). Indeed, no relationship between the microstructure of the weld and the initiation of fatigue cracking could be observed in Fig. 6.

As expected, fatigue test results in Fig. 4 show that higher partial pressures of CO_2 in the environment lead to reductions in the fatigue life of the specimen; this had been shown in literature (Ref 19-24), and is due to that fact that there is a rise in carbonic acid (H_2CO_3) concentration in the medium which causes an increase in corrosive processes and cathodic reaction rates. Figure 4 shows that a reduction of up to four times occurs in the corrosion-fatigue life of specimens tested in saline water with 103 kPa CO_2 in comparison with the "in air" condition. Further reduction in corrosion-fatigue life is seen when comparing the 103 kPa CO_2 condition with the 21 and 55 kPa conditions; arrows drawn in the graph help to highlight this. The continuous reduction of fatigue life as the CO_2 partial pressure increases is more noticeable for the high values of stress range; it can be observed from Fig. 4 and data in Table 3 that the corrosion-fatigue curve obtained in tests with 103 kPa CO_2 has a lower B coefficient than the other three curves. This indicates that the fatigue life reduction factor in higher CO_2 pressures is less marked when lower stresses are applied.

Extrapolation of corrosion-fatigue data for larger numbers of cycles may cause some concern. However, reaching millions of cycles at low frequencies is clearly extremely time-consuming, and estimations of the corrosion-fatigue life of specimens at higher numbers of cycles by extrapolation can be considered a reliable procedure if they are performed according to statistically sound procedures such as those outlined, for example, in ASTM E739 (Ref 27).

An explanation for the different inclination of the 103 kPa curve in comparison with the other curves (Fig. 4) may be the competition between crack growth and corrosion (Ref 1, 25). When small loads are applied, the fatigue crack growth rate is so small that there is a larger interaction time between the crack tip and the aggressive environment. If the corrosion associated with the environment is high enough, there would be anodic dissolution of the crack surfaces, leading to a blunting mechanism of the crack tip. A detailed study of such effects was presented in Ref 1, where crack propagation and corrosion rates were quantitatively estimated for different test configurations; in that work, a crack blunting effect was identified for specific combinations of CO_2 partial pressure, pH values, temperature, and NaCl concentration.

Besides this competition between corrosion rate and corrosion-fatigue crack propagation rate, literature describes a second interaction process which can also occur. This consists of the anodic dissolution of persistent slip bands (PSBs), which are microdeformations, typical of the fatigue crack initiation processes (Ref 16, 25). In higher loading conditions such as PSBs are deeper, resulting in higher roughness, and the time for crack nucleation is small compared with the time to eliminate them through superficial anodic dissolution (Ref 16, 25). That would explain why the fatigue life reduction factor is more substantial at higher stress ranges. On the other hand, at lower stress ranges the PSBs lead to less rough surfaces, which means that their anodic dissolution is faster, thus delaying the corrosion-fatigue crack nucleation (Ref 25). This phenomenon, however, was verified in grades of steel other the one analyzed in this study and in Ref 1.

5. Conclusions

In tests of API 5L X65 girth weld specimens in aqueous media with a chloride content of 115,000 ppm, at 35 °C, and saturated with varying CO_2 absolute partial pressures, corrosion fatigue of girth welds in environments containing 21 and 55 kPa of CO_2 partial pressures presented an unsurprising reduction of fatigue life in comparison with "in air" tests, with very similar S-N curves being registered for both cases. Results obtained in tests with a CO_2 concentration of 103 kPa showed a more marked reduction in corrosion-fatigue life at higher stress range levels in comparison with lower levels, where performance was closer to the lower CO_2 concentration cases. This phenomenon, which is similar to a "recovery" of fatigue endurance under certain conditions, was attributed to the existence of a competition between the corrosion rate and the processes of initiation and propagation of corrosion-fatigue cracks, which leads to blunter cracks. In all tests, the absence of microstructural influence on the crack nucleation was observed, the weld root toe being clearly the preferential site for such occurrence in all cases.

Acknowledgments

The authors would like to thank PETROBRAS and the CNPq and CAPES agencies of the Brazilian Government for support.

References

1. R. Pargeter, B. Holmes, and D. Baxter, Corrosion Fatigue of Steel Catenary Risers in Sweet Production, *Proceedings of the ASME 27th International Conference on Offshore Mechanics and Arctic Engineering (OMAE), 57075*, Vol 3, 2008, p 63–74
2. K.E. Szklarz, Aggressive CO_2 Corrosion and Fatigue Behavior of Pipeline Girth Welds, *Proceedings of Corrosion/2000, 00012*, NACE International, Houston, 2000
3. D.P. Baxter, S.J. Maddox, and R.J. Pargeter, Corrosion Fatigue Behaviour of Welded Risers and Pipelines, *Proceedings of the ASME 28th International Conference on Offshore Mechanics and Arctic Engineering (OMAE), 29360*, Vol 4, 2009, p 117–124
4. S.J. Maddox, R.J. Pargeter, and P. Woollin, Corrosion Fatigue of Welded C-Mn Steel Risers for Deepwater Applications: A State of the Art Review, *Proceedings of the ASME 24th International Conference on Offshore Mechanics and Arctic Engineering (OMAE), 67499*, Vol 3, 2005, p 245–251
5. E.S. da Silva, M.A.N. Beltrão, and F.L. Bastian, Comportamento em fadiga de juntas soldadas circunferenciais de um aço API 5L X80, *18nd Brazilian Conference of Materials Science and Engineering (in Portuguese), 312-040*, 2008
6. A. Fragiel, S. Serna, B. Campillo, and L. Cota, Dissimilar Mechanical Properties—Microstructures Microalloyed Pipeline Steels Cracking Performance Under Sour Environment, *Mater. Sci. Eng. A*, 2007, **467**, p 1–7
7. F. P. dos Santos, "Desenvolvimento de ensaios de corrosão fadiga para juntas soldadas de aço API 5l X60," M.Sc. Thesis (in Portuguese), Post-Graduation Program in Mining, Metallurgical and Materials Engineering, Federal University of Rio Grande do Sul, Brazil, 2006
8. P. Woollin, R.J. Pargeter, and S.J. Maddox, Corrosion Fatigue Performance of Welded Risers for Deepwater Applications, *Proceedings of Corrosion/2004, 04144*, NACE International, Houston, 2004
9. American Petroleum Institute, API 5L, Specification for Line Pipe, 2004
10. M. Cohen and S.S. Hansen, Microstructural Control in Microalloyed Steels, MiCon 78: Optimization of Processing, Properties and Service Performance Through Microstructural Control, ASTM Special Technical Publication 672, 1979, p 34–52
11. J.Q. Wang, A. Atrens, D.R. Cousens, and N. Kinaev, Microstructures of X52 and X65 Pipeline Steels, *J. Mater. Sci.*, 1999, **34**, p 1721–1728
12. F.G. Perini, "Propriedades mecânicas e microestruturais de aços de alta resistência e baixa liga," M.Sc. Thesis (in Portuguese), Post-Graduation Program in Materials Science, University of Caxias do Sul, Brazil, 2008
13. Offshore Standard, DNV-OS-C401, Fabrication and Testing of Offshore Structures, Det Norske Veritas, 2004
14. W.C. Lyons, *Standard Handbook of Petroleum & Natural Gas Engineering*, ISBN 0-88415-643-5, Gulf Professional Publishing, 1996
15. K.A. MacDonald and S.J. Maddox, New Guidance for Fatigue Design of Pipeline Girth Welds, *Eng. Fail. Anal.*, 2003, **10**, p 177–197
16. J. Schijve, Fatigue of Structures and Materials in the 20th Century and the State of the Art, *Int. J. Fatigue*, 2003, **25**, p 679–702
17. V. Lawrence, N.J. Ho, and P.K. Mazumdar, Predicting the Fatigue Resistance of Welds, *Ann. Rev. Mater. Sci.*, 1981, **11**, p 401–425
18. I. Lotsberg, Stress Concentration Factors at Welds in Pipe Lines and Tanks Subjected to Internal Pressure and Axial Force, *Mar. Struct.*, 2008, **21**, p 138–159
19. T. Li, Y. Yang, K. Gao, and M. Lu, Mechanism of Protective Film Formation During CO_2 Corrosion of X65 Pipeline Steel, *J. Univer. Sci. Technol. Beijing*, 2008, **15**(6), p 702–711
20. S. Nešić, Key Issues Related to Modelling of Internal Corrosion of Oil and Gas Pipelines—A Review, *Corros. Sci.*, 2007, **49**, p 4308–4338
21. K. Gao, F. Yu, X. Pang, G. Zhang, L. Qiao, W. Chu, and M. Lu, Mechanical Properties of CO_2 Corrosion Product Scales and Their Relationship to Corrosion Rates, *Corros. Sci.*, 2008, **50**, p 2796–2803
22. D.A. López, T. Pérez, and S.N. Simison, The Influence of Microstructure and Chemical Composition of Carbon and Low Alloy Steels in CO_2 corrosion. A State-of-the-Art Appraisal, *Mater. Des.*, 2003, **24**, p 561–575
23. A.F. Razi, A. Pendashteh, L.C. Abdullah, D.R.A. Biak, S.S. Madaeni, and Z.Z. Abidin, Review of Technologies for Oil and Gas Produced Water Treatment, *J. Hazard. Mater.*, 2009, **170**(2-3), p 530–551
24. L. Smith, Control of Corrosion in Oil and Gas Production Tubing, *Br. Corros. J.*, 1999, **34**, p 247–253
25. A. Gironès, A. Mateo, L. Llanes, M. Anglada, J. Deluccia, and C. Laird, Evaluation of Fatigue Damage for Duplex Stainless Steels in

Aggressive Environments by Means of an Electrochemical Fatigue Sensor (EFS), *Int. J. Fatigue*, 2003, **25**, p 1189–1194
26. American Society for Testing and Materials, ASTM E468, Presentation of Constant Amplitude Fatigue Test Results for Metallic Materials, 2004
27. American Society for Testing and Materials, ASTM E739, Statistical Analysis of Linear or Linearized Stress-Life (S-N) and Strain-Life (ε-N) Fatigue Data, 2004
28. E.P. Popov, *Mechanics of Materials*, 2nd ed., Prentice Hall, New Jersey, 1976
29. A.P. Jivkov, Evolution of Fatigue Crack Corrosion from Surface Irregularities, *Theor. Appl. Fract. Mech.*, 2003, **40**, p 45–54
30. British Standard, BS 7608, Code of Practice for Fatigue Design and assessment of Steel Structures, 1993
31. M.C. Branco, A.A. Fernandes, and P.T. de Castro, *Fadiga de estruturas soldadas*, 1st ed., Fundação Calouste, Porto, Portugal, 1986